
Supplementary information

Strong control of effective radiative forcing by the spatial pattern of absorbing aerosol

In the format provided by the
authors and unedited

Supplementary material for “Strong control of effective radiative forcing by the spatial pattern of absorbing aerosol”

Andrew I. L. Williams^{1*}, Philip Stier¹, Guy Dagan², Duncan Watson-Parris¹

¹Atmospheric, Oceanic and Planetary Physics, Department of Physics, University of Oxford, UK

²Fredy and Nadine Herrmann Institute of Earth Sciences, The Hebrew University of Jerusalem, Jerusalem, Israel

*Correspondence to: Andrew Williams (andrew.williams@physics.ox.ac.uk)

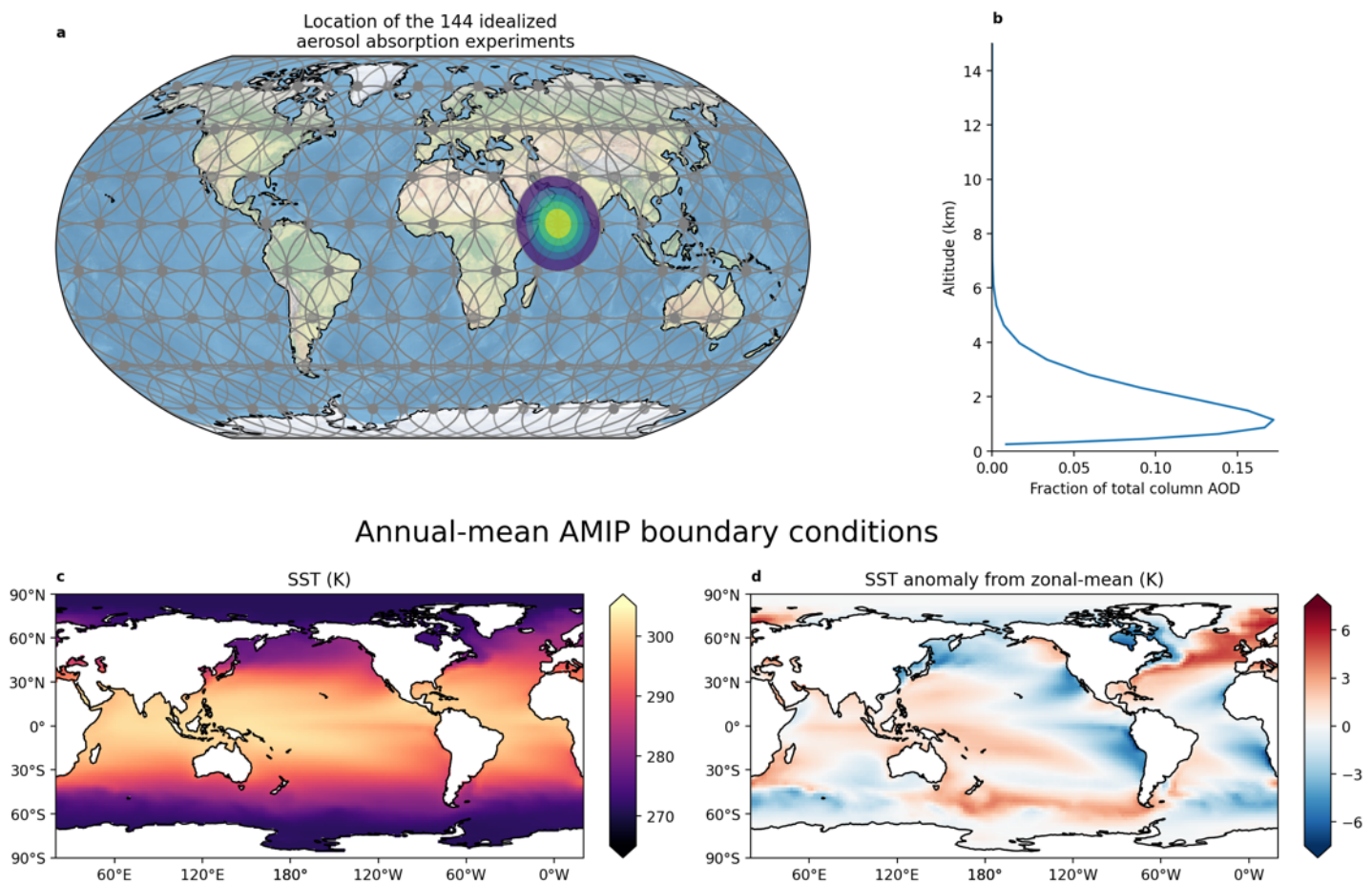


Figure 1: **a** Geographic illustration of the 144 idealized aerosol plumes used. Grey ellipses illustrate the extent of the plume in each experiment. Each plume corresponds to a separate experiment and a filled contour illustrating the horizontal structure of the plume AOD is shown for the plume centered over the Indian Ocean. **b** Vertical profile of fractional aerosol optical depth at 533nm with respect to the column integral. The vertical axis denotes the approximate altitude above the local surface. The vertical profile is constant for all the perturbation experiments we conduct. **c, d** Annual-mean SST field used to drive the simulations, along with the corresponding SST anomaly relative to the zonal-mean temperature.

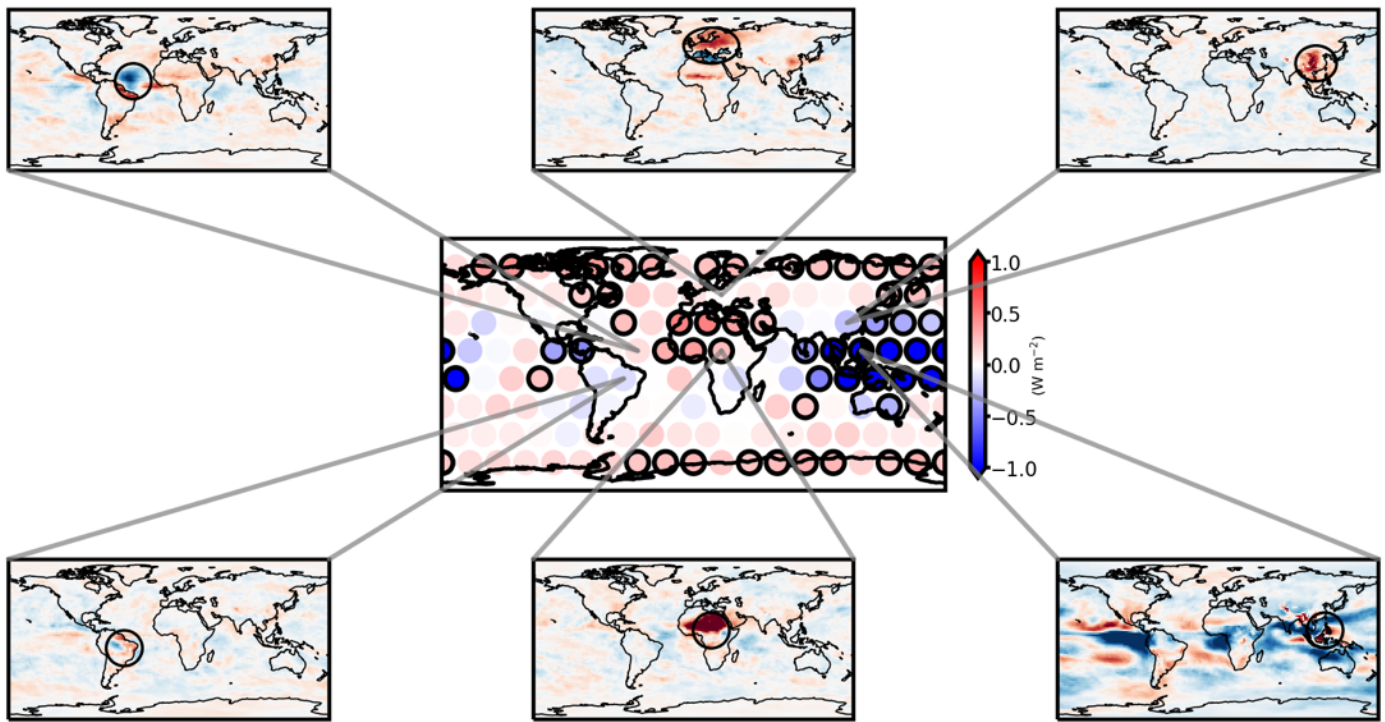


Figure 2: As in Figure. 1, except showing the spatial pattern of time-mean ERF for six other representative AA perturbation sites. The colours in each of the insets become saturated at $\pm 10\text{Wm}^{-2}$.

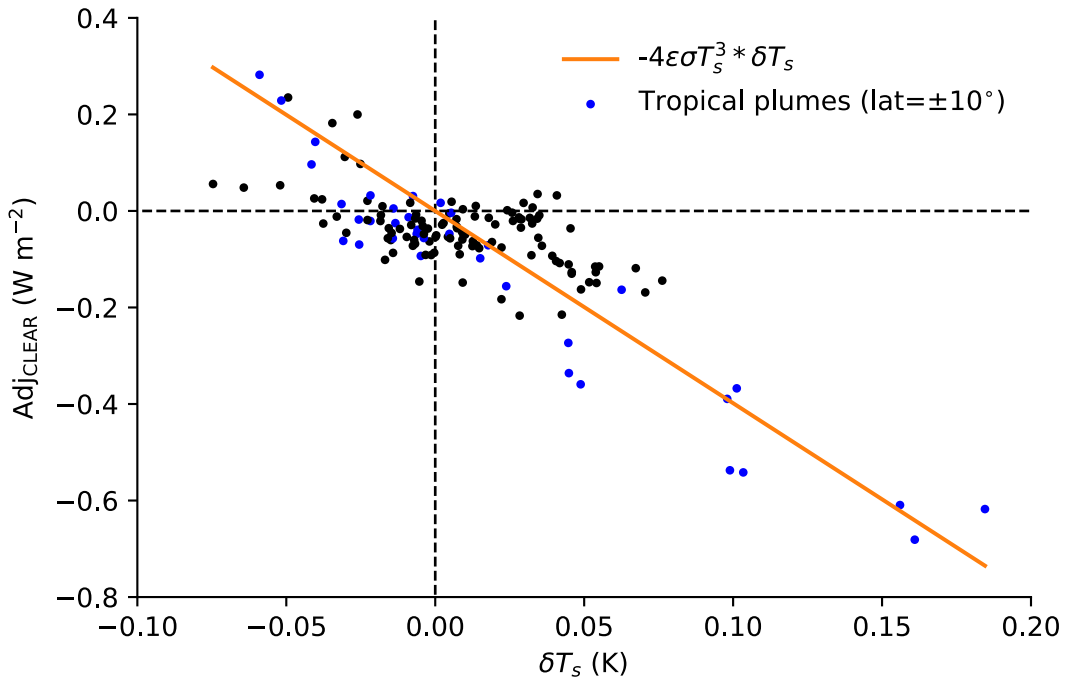


Figure 3: Scatter plot of global-mean changes in clear-sky rapid adjustments versus global-mean surface temperature changes for each of the 144 plume experiments. Tropical plumes (i.e., those with their central latitude at $\pm 10^\circ$) are coloured in blue and a parameter-free prediction of the slope (given by Equation 2 in Methods) is drawn in orange.

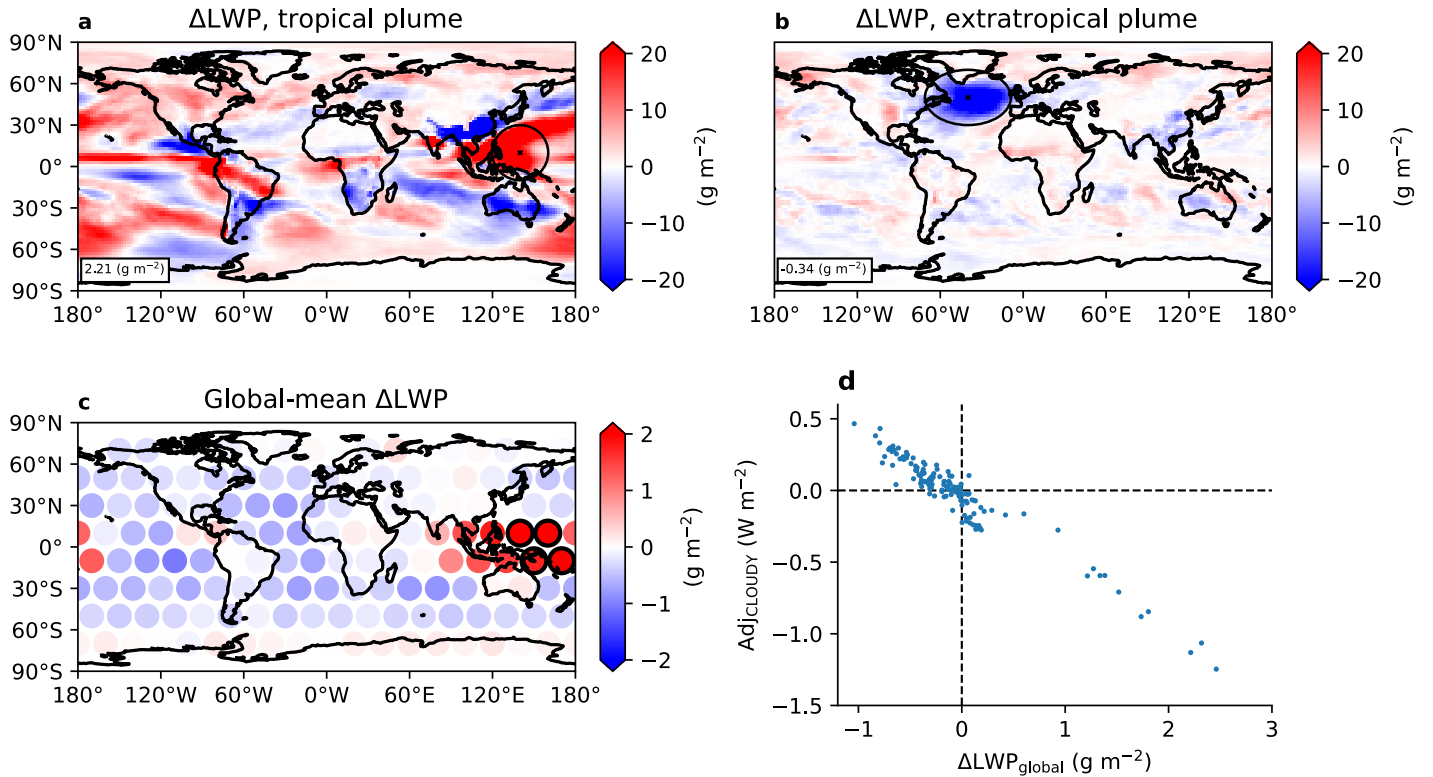


Figure 4: **a** Time-mean liquid water path (LWP) changes for the simulation with the idealized aerosol plume located over the Southern Indian Ocean and **b** the idealized aerosol plume located over the North Atlantic. The text box shows the value of the global-mean LWP change in each case. **c** Global-mean changes in LWP resulting from idealized aerosol plumes in different locations. **d** shows a scatter plot of the global-mean cloudy-sky adjustments versus the global-mean LWP changes in each of the experiments, demonstrating the strong control of $\text{Adj}_{\text{cloudy}}$ by LWP.

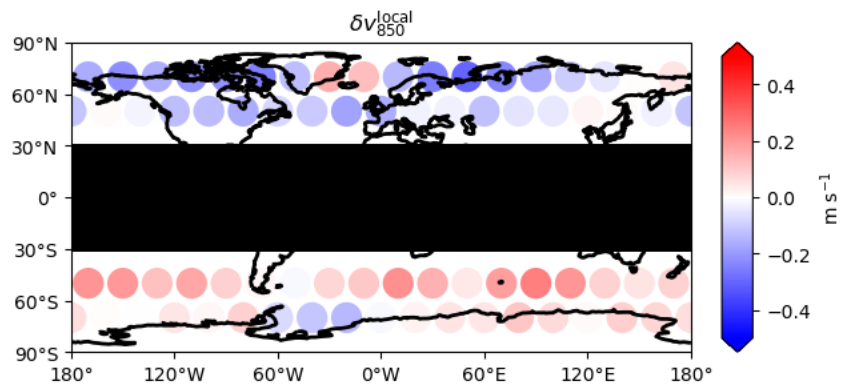


Figure 5: Local- and time-mean changes in the meridional velocity at 850hPa for each of the experiments where the AA perturbation was in the midlatitudes. Blue colours indicate anomalous southwards flow (equatorward in the NH) in response to aerosols, and red colours indicate anomalous northwards flow (equatorward in the SH) in response to the aerosols.

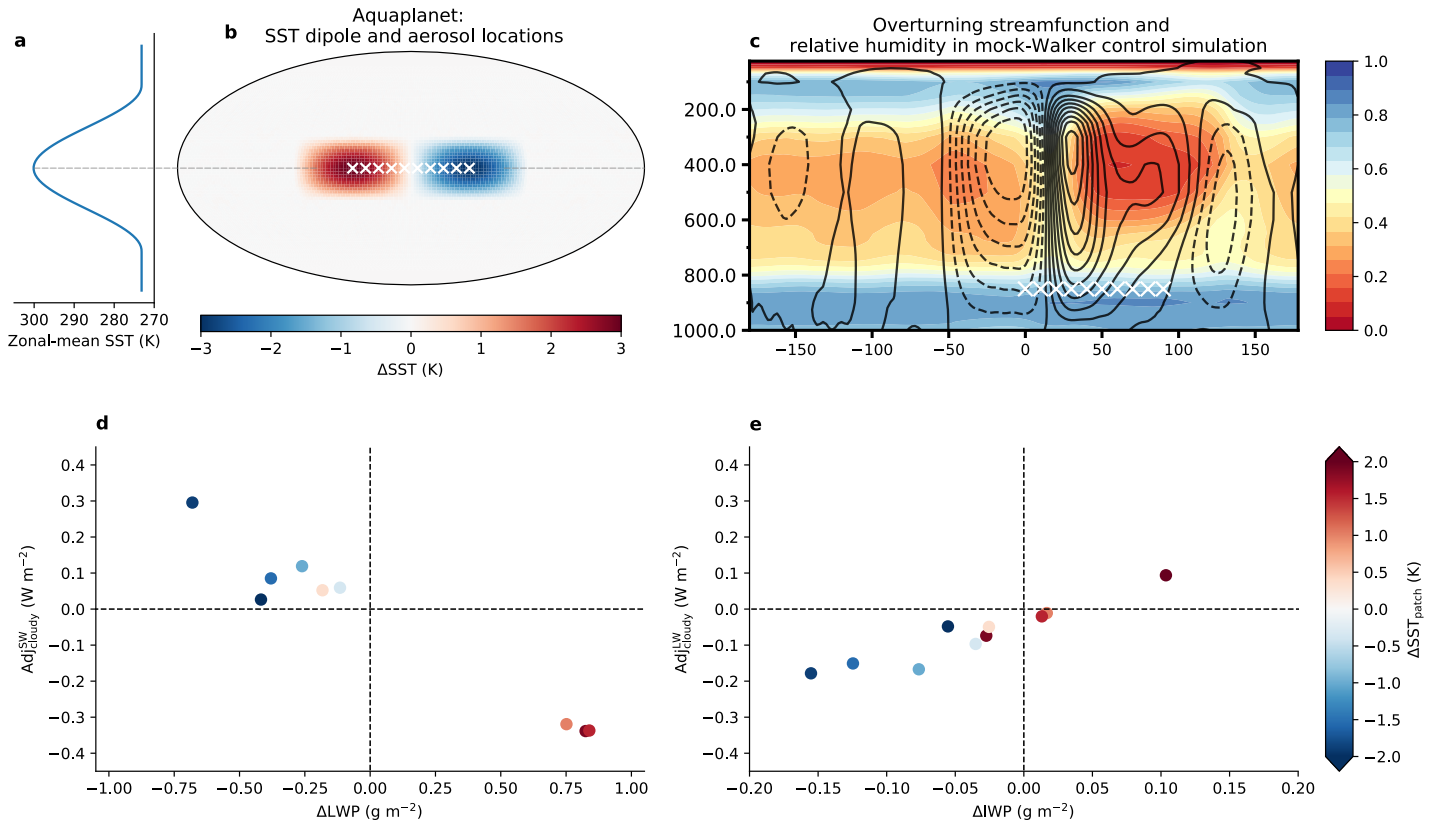


Figure 6: Overview of the mock-Walker aquaplanet simulations. **a** The zonal-mean SST profile prescribed in the model. **b** The zonally-anomalous SST dipole imposed along the equator, with white markers illustrating the location of the 10 aerosol absorption experiments conducted. **c** Pressure-longitude plot of the relative humidity (colours) and zonal mass streamfunction (black contours) averaged between $\pm 20^\circ$ of the equator with area-weighting in the control simulation. The white markers show the approximate longitude and pressure of the AOD maxima in the 10 perturbation experiments. **d** The shortwave component of the global-mean cloudy-sky adjustments in each of the 10 experiments scattered against the global-mean LWP change. **e** The longwave component of the global-mean cloudy-sky adjustments in each of the 10 experiments scattered against the global-mean IWP change. In panels **d** and **e** the colour of the markers illustrates the SST anomaly (from **b**) at the center of the plume in each experiment.

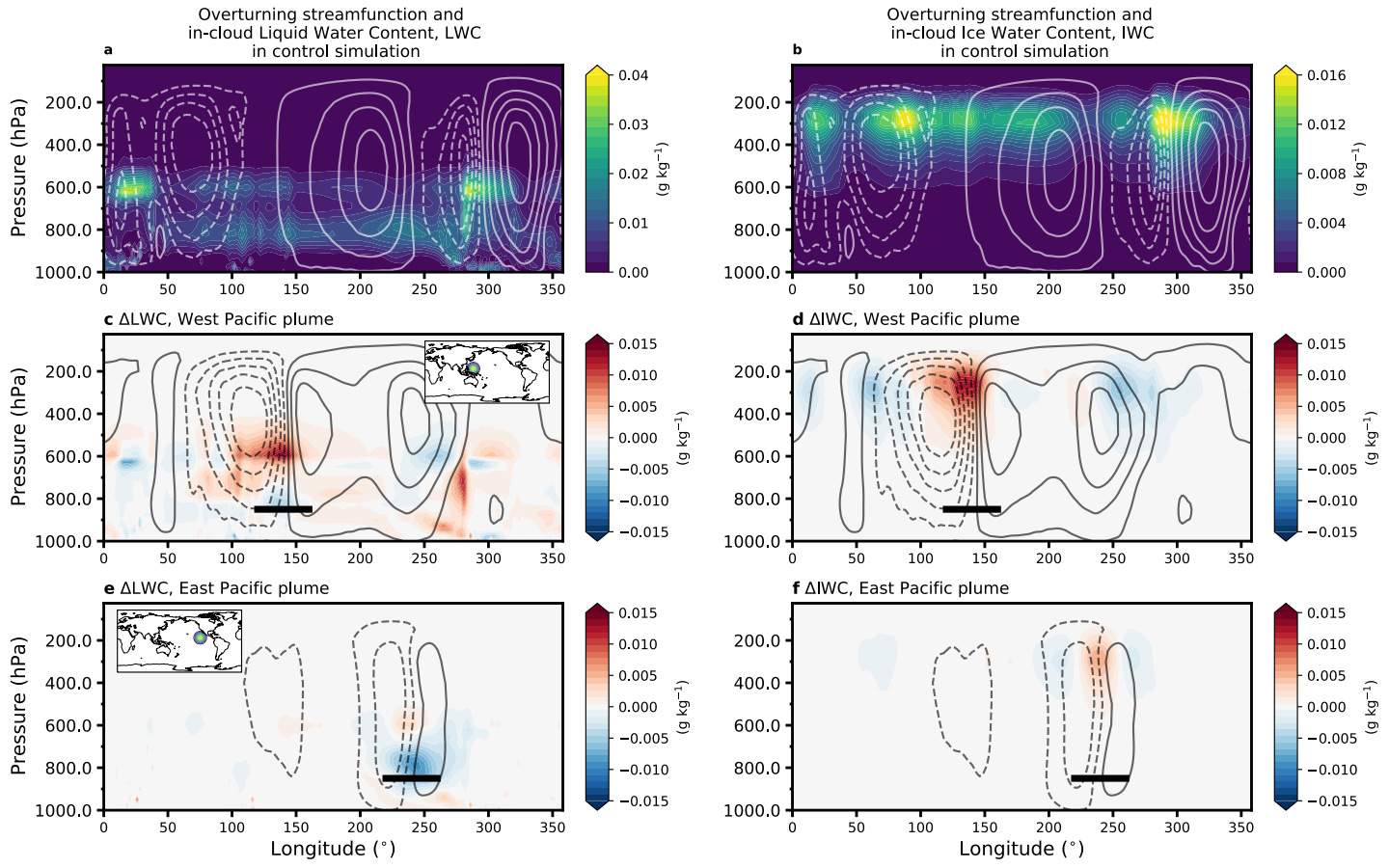


Figure 7: Cloud liquid and ice water content in the control simulations (a, b) and changes in response to plumes in the East and West Pacific. Contours indicate the zonal mass stream-function in the control simulation (a, b) and changes in the stream-function are shown in (c, d, e, f). Solid contours indicate clockwise motion. In the lower two rows, horizontal black lines illustrate the 2-sigma (40°) horizontal extent of the plume, at a height corresponding roughly to the maximum of the plume AOD profile.

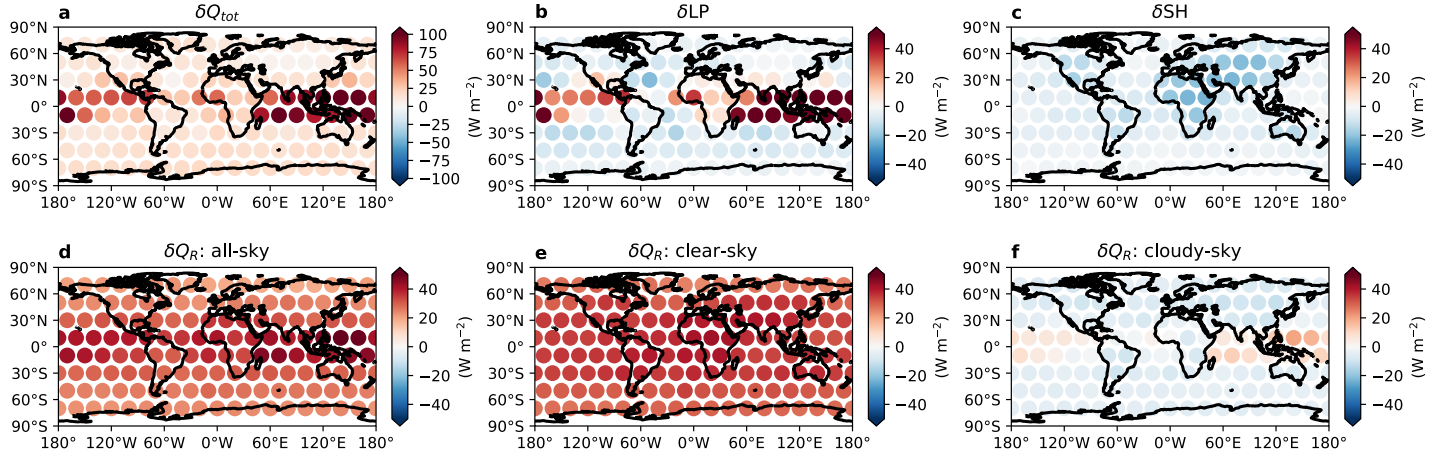


Figure 8: **a** The local diabatic heating anomaly in each of the experiments, and contributions from **b** precipitation feedbacks, **c** sensible heat flux changes, **d** atmospheric radiative cooling. Panels **e** and **f** show the decomposition of atmospheric radiative cooling into contributions from clear and cloudy sky, respectively.

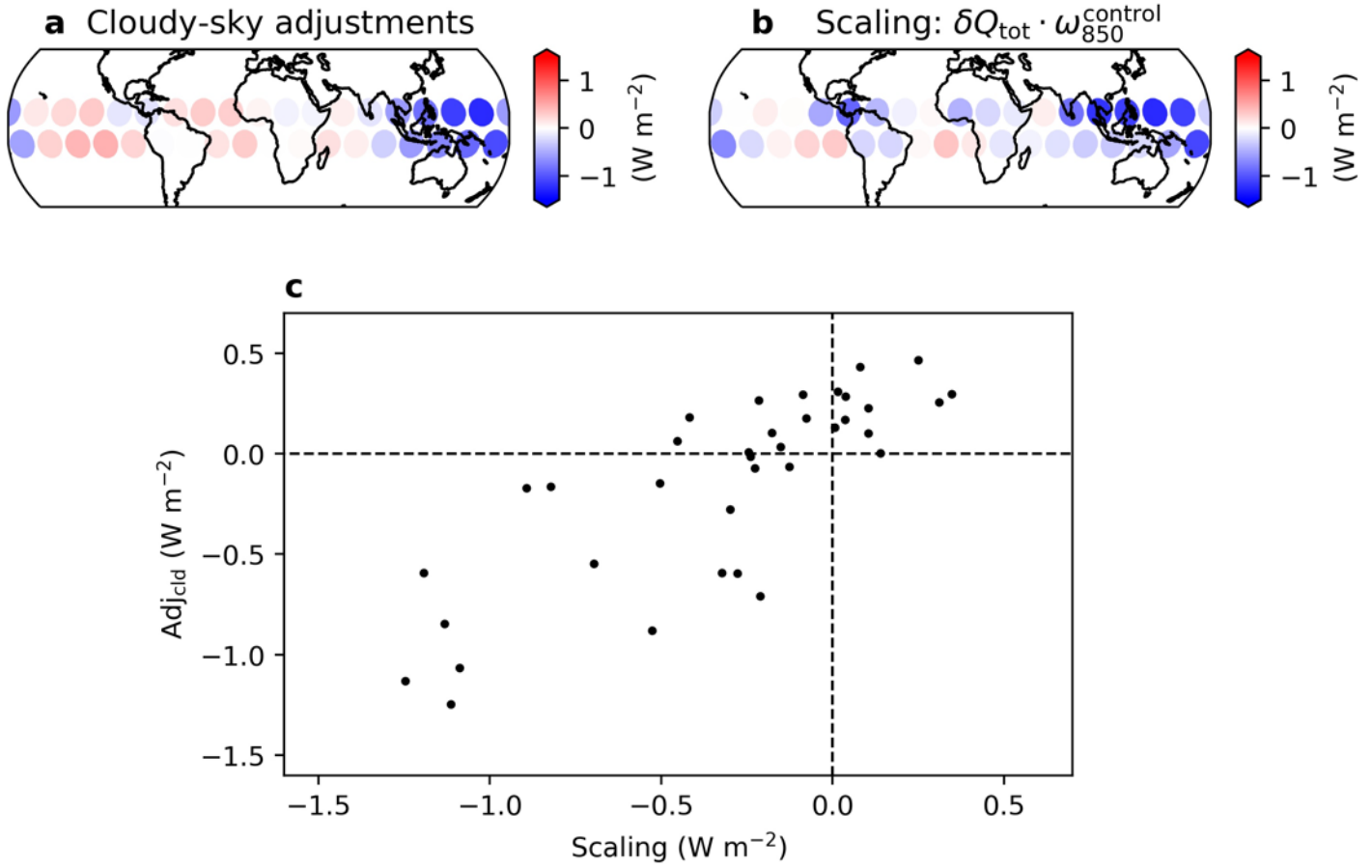


Figure 9: As in Fig. 4 but using the local vertical velocity at 850hPa instead of the difference between the horizontal divergence between 850hPa and 400hPa. This scaling still captures much of the variation in cloudy-sky adjustments in response to AAs throughout the tropics and the strong negative ERF in response to AAs over the Western tropical Pacific, however it overestimates the response over tropical land.

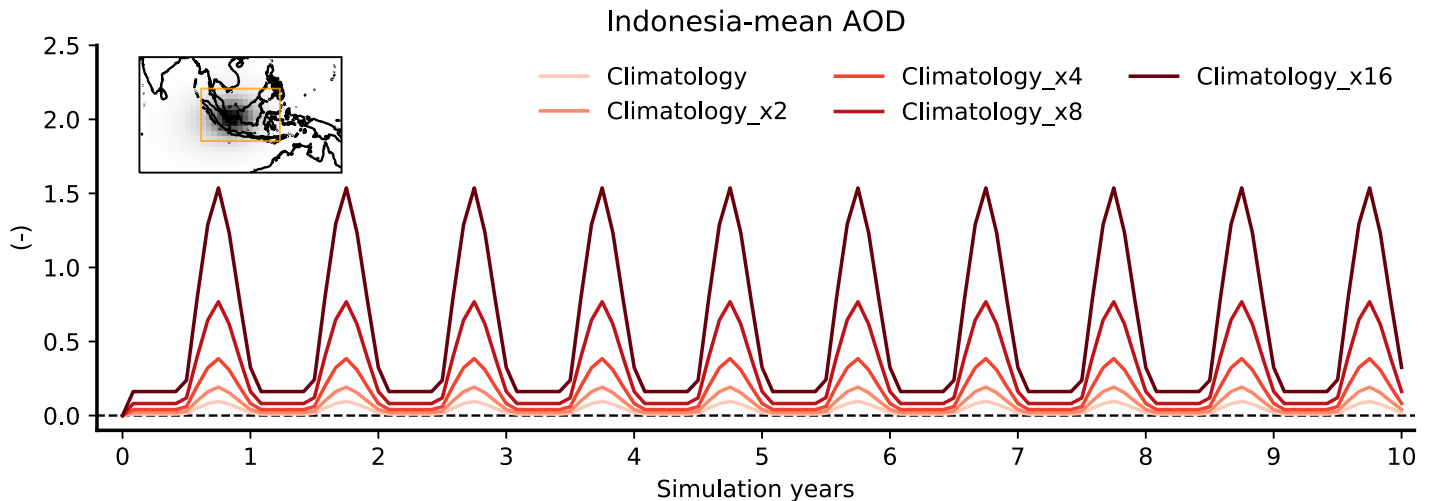


Figure 10: Time-series of Indonesia-mean AOD in our experiments with the realistic climatology of Indonesian biomass-burning, with a seasonal cycle which peaks in the dry-season (Methods). The orange box in the inset shows the averaging area and encompasses the same area as the inset in Fig. 5 of the main article. For each experiment we double the AOD relative to the climatological distribution.

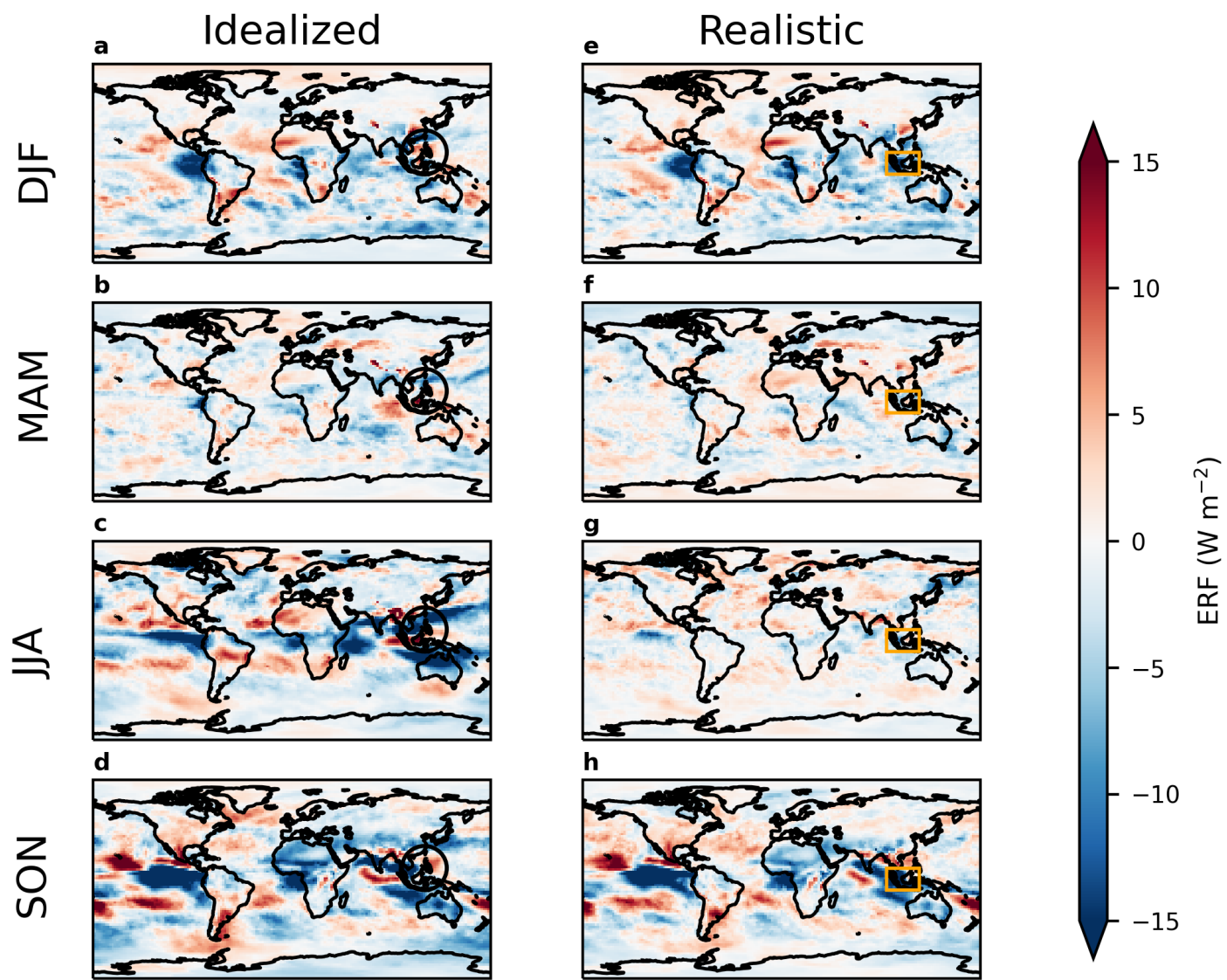


Figure 11: Seasonal-mean ERF response for the idealized (a,b,c,d) and realistic (e,f,g,h) AA perturbations over Indonesia.

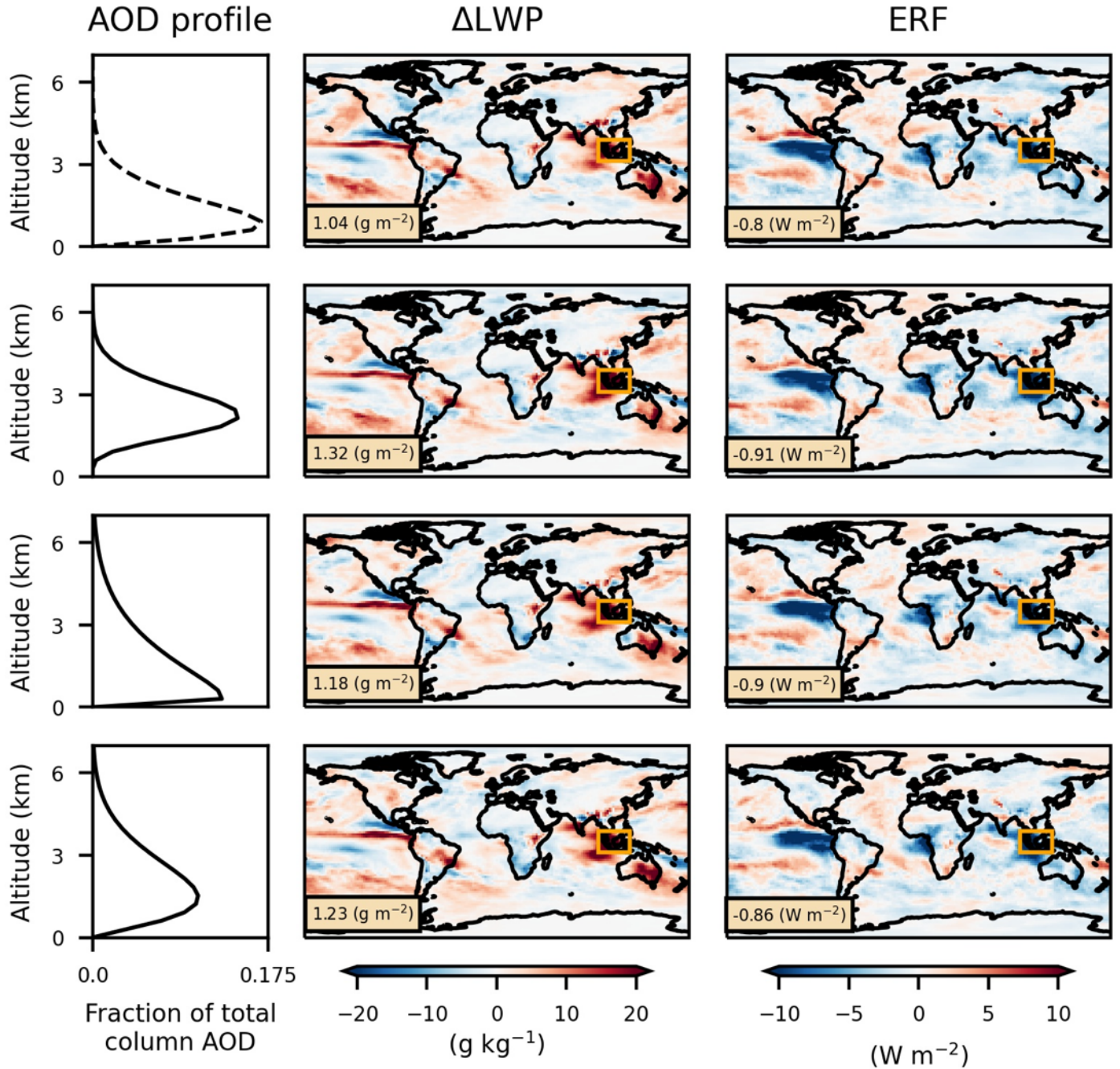


Figure 12: Top-row shows the vertical aerosol profile used in the ‘Climatology_x16’ Indonesian wildfire experiment (dashed line, top-left), along with the change in LWP and the ERF in the middle and right columns. Each row below this corresponds to the same ‘Climatology_x16’ experiment, except we have varied the vertical aerosol profile to sample realistic variability in the vertical structure of the perturbation. This figure shows that our main results regarding the Indonesia wildfire experiment are not sensitive to realistic variations in the vertical profile.

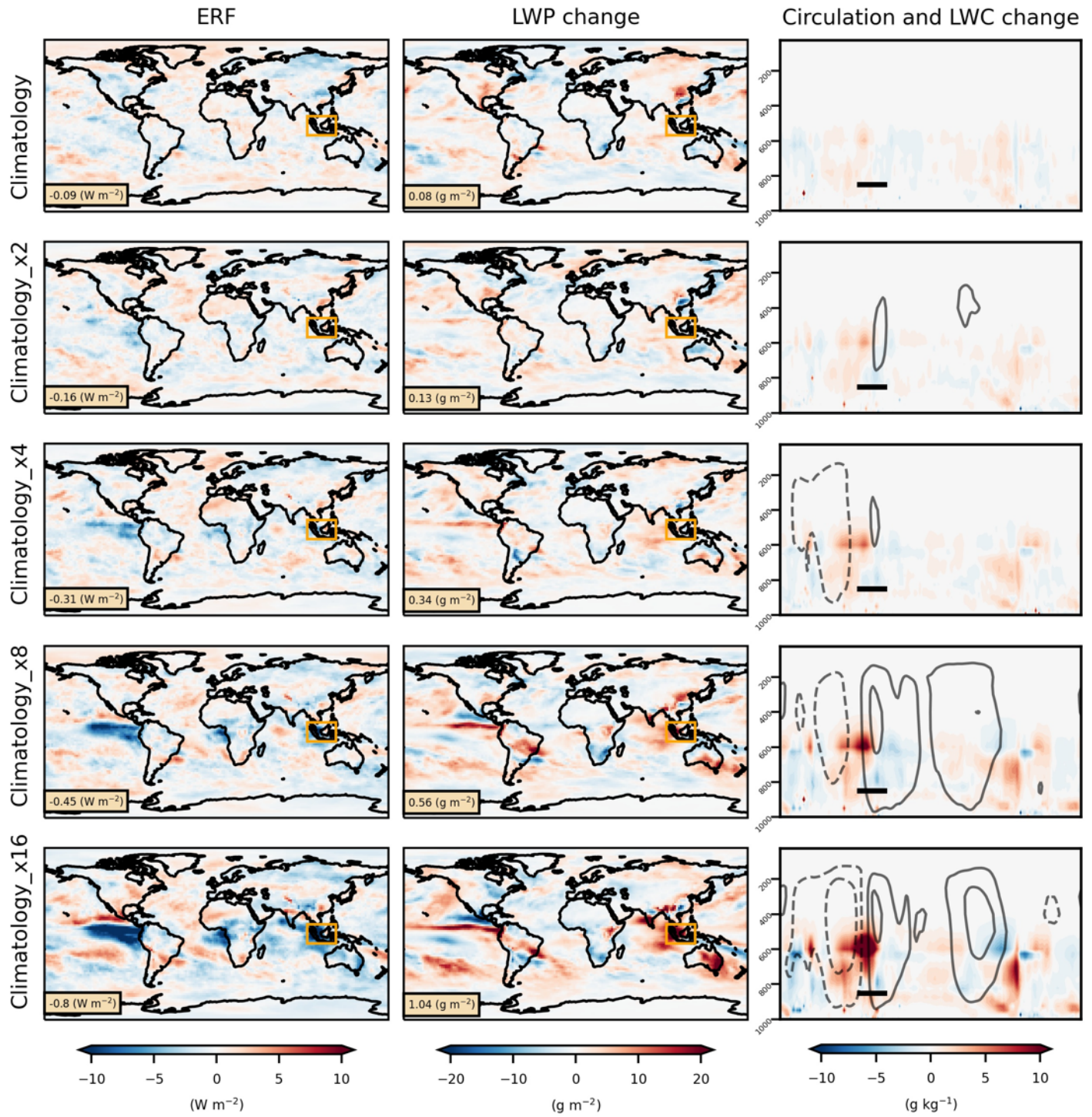


Figure 13: Annual-mean Effective Radiative Forcing (ERF), in-cloud Liquid Water Path (LWP), Liquid Water Content (LWC) and zonal-mass stream function changes in response to the five Indonesian biomass burning experiments compared to the control experiment with no AOD. The left column shows the ERF in each of the successive doubling experiments outlined in Fig. S9, with the global-mean ERF presented in the corner of each panel. The middle column shows the LWP changes in each of the experiments, illustrating again that the ERF and the LWP are highly anti-correlated. The rightmost panel shows pressure-longitude cross-sections of the in-cloud liquid water content (LWC, colours) and zonal mass stream-function (contours) in the control simulation, averaged 20° either side of the equator in each experiment - same plotting conventions as in Fig. 2 of the main article. In the right column, horizontal black lines illustrate the horizontal extent of the AOD perturbation, at a height corresponding roughly to the maximum of the plume AOD profile (see Methods).